Tracking Exceptional Points above Laser threshold in Nanolasers Supplementary Materials

Kaiwen Ji,[1] Qi Zhong,[2] Li Ge,[3] Gregoire Beaudoin,[1] Isabelle Sagnes,[1] Fabrice Raineri,[1] Ramy El-Ganainy,[2,4] and Alejandro Giacomotti[1]

[1]Centre de Nanosciences et de Nanotechnologies, CNRS, Université Paris-Saclay, 10 Boulevard Thomas Gobert, 91120 Palaiseau, France
[2]Department of Physics, Michigan Technological University, Houghton, Michigan 49931, USA
[3]Department of Physics and Astronomy, College of Staten Island, CUNY, Staten Island, New York 10314, USA and the Graduate Center, CUNY, New York, New York 10016, USA
[4]Henes Center for Quantum Phenomena, Michigan Technological University, Houghton, Michigan 49931, USA

S1. COMPENSATING THE CARRIER-INDUCED FREQUENCY DETUNING

As we mentioned in the main text, under asymmetric pumping of the two resonators, the carrier-induced frequency shift (which is proportional to the linewidth enhancement factor α) will break the parity symmetry between the two resonators. As a result, it is not possible to achieve PT symmetry and access the EP. In order to compensate for this dynamic effect, the two cavities must be designed to be initially asymmetric, i.e. having two different resonant frequencies. If the detuning is properly chosen, it can counterbalance the effect of the dynamic frequency shift. Here we derive the required frequency detuning to achieve this target. To do so, we start by considering the field equations of the laser rate model of Eq.(1a) in the main text, which can be expressed in the form:

$$-i\frac{d}{dt}\begin{bmatrix}a_1\\a_2\end{bmatrix} = H_{NL}\begin{bmatrix}a_1\\a_2\end{bmatrix} \tag{S1}$$

where

$$H_{NL} = \begin{bmatrix}(\omega_1+\Delta\omega_1)-ig_1 & K\\ K & (\omega_2+\Delta\omega_2)-ig_2\end{bmatrix},$$

$\Delta\omega_j = \frac{\alpha}{2}(n_j-n_0)\beta\Gamma_{\parallel}$ and $g_j = -\kappa + (n_j-n_0)\beta\Gamma_{\parallel}/2$, with $j = 1,2$. Before we proceed, we emphasize the fact that the above equations incorporate the nonlinear effects arising from the coupling between the carrier and intensity. In other words, no linear approximations are made here. By expressing the fields as $a_j = A_j e^{i\phi_j} e^{i\Omega t}$ with A_j and ϕ_j being real numbers, we arrive at:

$$\Omega_{\pm} = \omega_{avg} - ig_{avg} \pm \sqrt{K^2 - \frac{(i\delta\omega_{12}+i\Delta\omega_{12}+\Delta g_{12})^2}{4}} \tag{S2}$$

where $\omega_{avg} \equiv (\omega_1+\omega_2+\Delta\omega_1+\Delta\omega)/2$, $g_{avg} \equiv (g_1+g_2)/2$, $\Delta\omega_{12} \equiv \Delta\omega_1 - \Delta\omega_2 = \frac{\alpha}{2}(n_1-n_2)\beta\Gamma_{\parallel}$, $\Delta g_{12} \equiv g_1 - g_2$, and finally $\delta\omega_{12} \equiv \omega_1 - \omega_2$.

In order to steer the system to an EP, the following two conditions must be satisfied: (i) $\delta\omega_{12} = -\Delta\omega_{12}$, (ii) $\Delta g_{12}/2 = K$. In writing this last relation, we assumed that $n_1 > n_2$ since here $K > 0$. Obviously, the other choice could have been made as well. Taken together, these two conditions lead to

$$\delta\omega_{12} = -2K\alpha. \tag{S3}$$

Importantly, since the lasing frequencies, $\Omega_{\pm}$ must be real, we find that at the EP (in fact even for $K > \Delta g_{12}$) $g_{avg} = 0$, or equivalently $g_1 = -g_2$. In other words, at the EP, the system respects PT symmetry.

In order to confirm the validity of this analysis, we have calculated the lasing modes of two asymmetric laser cavities under the above derived detuning conditions. Figure.S1 plots the resultant bifurcation diagrams for different values of α and the corresponding detuning. For both cases, effective PT symmetry is resorted at the branch points, which suggests that the compensation scheme described above can work under a wide range of parameters.

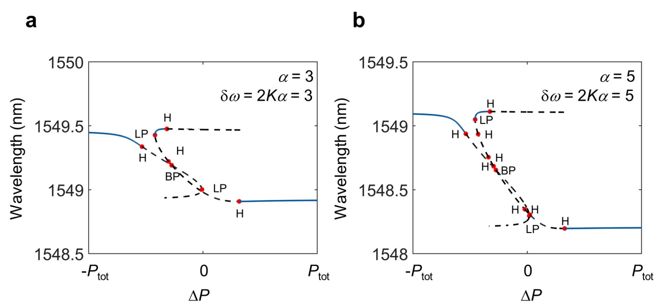

FIG. S1. Compensation of nonlinearity for different α values. $K = 0.5, P_{tot} = 3P_0$

S2. LOCATING THE EP IN THE PARAMETER SPACE

In this note, we derive the condition for operating at an EP above he lasing threshold. To do so, we start by recalling the characteristics of a lasing EP, which can be summarized as follows: (i) $\delta\omega = 2K\alpha$, (ii) $g_1 = -g_2$, (iii) The fields in both cavities have equal amplitude, and (iv) The phases of the fields in both cavities are different by a factor of $\pi/2$. As discussed before, the first of these conditions is the frequency detuning required to compensate for the carrier-induced frequency shift at the EP. When this condition is satisfied, the second relation becomes the lasing condition (imaginary part of $\Omega_\pm = 0$) at the EP. The third and forth arise directly from the expression for the exceptional eigenvector associate with the solution of matrix eigenvalue problem in Eq.(S1). In other words, we have:

$$\frac{1}{2}(n_1 - n_0)\beta\Gamma_\parallel - \kappa = -\left[\frac{1}{2}(n_2 - n_0)\beta\Gamma_\parallel - \kappa\right] \tag{S4}$$

$$\frac{\alpha}{2}(n_1 - n_0)\beta\Gamma_\parallel = \frac{\alpha}{2}(n_2 - n_0)\beta\Gamma_\parallel + 2K\alpha \tag{S5}$$

$$|a_1|^2 = |a_2|^2, \tag{S6}$$

$$\phi_1 - \phi_2 = \pi/2. \tag{S7}$$

By solving Eqs. (S4) and (S5), we can obtain the following expressions for the carrier numbers at EP:

$$n_1 = n_0 + \frac{2(K+\kappa)}{\beta\Gamma_\parallel}, \tag{S8}$$

$$n_2 = n_0 - \frac{2(K-\kappa)}{\beta\Gamma_\parallel}. \tag{S9}$$

Meanwhile, these carrier numbers can be related to the pump rates by solving the carrier rate equations (Eq.(1.b) in the main text) under steady states conditions, i.e., $\dot{n_1} = \dot{n_2} = 0$. By doing so, we arrive at:

$$P_j - n_j\Gamma_{tot} = (n_j - n_0)\beta\Gamma_\parallel |a_j|^2, \tag{S10}$$

From Eq. (S6) and Eq. (S10) we obtain:

$$\frac{n_1 - n_0}{n_2 - n_0} = \frac{P_1 - \Gamma_{tot} n_1}{P_2 - \Gamma_{tot} n_2}. \tag{S11}$$

Finally, by combining Eqs. (S9), (S10) and (S11), we obtain:

$$\Delta P|_{EP} = \frac{K(P_{tot} - 2n_0\Gamma_{tot})}{\kappa} \tag{S12}$$

where as in the main text, $\Delta P = P_1 - P_2$. Note that the sign in front of the left hand side is a result of the assumption $n_1 > n_2$ and the definition of ΔP. Recalling the definition of the gain difference at EP $\Delta g_{2,1}|_{EP} = \beta\Gamma_\parallel(n_2 - n_1)/2 = 2K$, we can rewrite Eq. (S12) as

$$\Delta P|_{EP} = -\frac{\Delta g_{2,1}|_{EP}(P_{tot} - 2n_0\Gamma_{tot})}{2\kappa}, \tag{S13}$$

which shows that the pump difference at the exceptional point, $\Delta P|_{EP}$, is not only a function of the gain difference, but also of the total pump power. At the laser threshold, it takes the simple form $\Delta P|_{EP}^{th} = (P_2 - P_1)|_{EP}^{th} = 2\Delta g_{2,1}\Gamma_{tot}/\beta\Gamma_\parallel$, which recovers the linear case.

On the other hand, to have EP in the strong pumping regime, Eq. (S12) must satisfy $\Delta P|_{EP} \leq P_{tot}$. In the high pumping limit it reduces to

$$\lim_{P_{tot}\to\infty} \frac{\Delta P_{EP}}{P_{tot}} = \frac{K}{\kappa}, \tag{S14}$$

which implies that the system parameters must satisfy the condition $K < \kappa$, i.e. the coupling between the two cavities must be smaller than the loss factor of each cavity. Note that the condition $K < \kappa$ also arises from the less restrictive requirement of $n_{1,2} > n_0$, together with $K, \kappa > 0$, as can be seen from Eqs. (S8) and (S9).

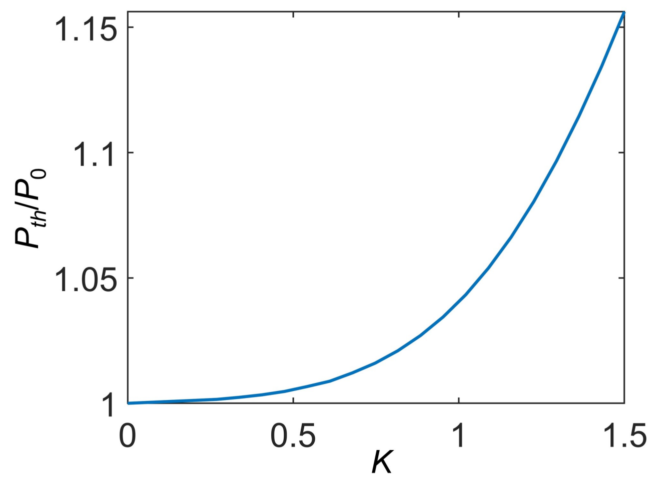

FIG. S2. Threshold of the broken PT phase.

Finally, let us consider the extreme case where the EP is approached when one of the cavities is pumped, namely $\Delta P|_{EP} = 1$ with $P_1 = P_{tot} = P_{EP}^{th}$, $P_2 = 0$ and $|a_1|^2 = |a_2|^2 = 0$. In this case, the values of gain coefficients in both cavities are given by $g_1 = -\kappa + \frac{1}{2}(n_1 - n_0)\beta\Gamma_\parallel$ and $g_2 = -\kappa - \frac{1}{2}n_0\beta\Gamma_\parallel$. The second of these formulas is a result of the fact that the steady state solution for the carrier in the second cavity (see Eq.(1b) in the main text) under the conditions $P_2 = 0$ and $|a_2|^2 = 0$ is $n_2 = 0$. Note that the expression for g_2 indicates that cavity 2 is actually experiencing net loss. In fact this is the maximum possible loss, which partly due to optical loss and partly due to absorption in the QW layer. On the other hand, as we discussed before, the condition for lasing at an EP is $g_1 = -g_2 = K$. By combining these results together, it becomes obvious that the EP cannot be accessed above the laser threshold if $K > \kappa + \frac{1}{2}n_0\beta\Gamma_\parallel$. For the parameters used in out work (see SM note 6 for a full list of parameters), this becomes $K/\kappa = 3.12$.

S3. LASING THRESHOLD AND FREQUENCY AT EP

At threshold, we have $|a_1|^2 = |a_2|^2 = 0$. From Eq. (S10), we thus obtain:

$$P_j^{th} = n_j\Gamma_{tot}. \tag{S15}$$

By using Eqs. (S8) and (S9), find:

$$P_{EP}^{th} = P_1^{th} + P_2^{th} = 2(n_0 + \frac{2\kappa}{\beta\Gamma_\parallel})\Gamma_{tot} = 2P_0, \tag{S16}$$

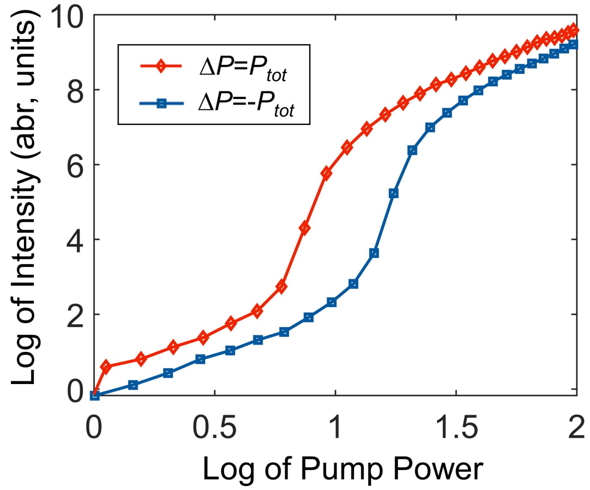

FIG. S3. Threshold of the of the system when a single cavity is pumped.

where P_0 is the threshold of the single cavity laser. This last relation confirms that $P_{tot} > 2n_0\Gamma_{tot}$ above the lasing threshold, which as expected results in a negative value for ΔP_{EP} (See Eq.(S12)). To complete the discussion, we have also evaluated the lasing threshold in the broken PT phase when $\Delta P = -1$ numerically as a function of the coupling coefficient K. This result is shown in Fig. S2.

To determine the lasing frequency at EP, we recall that at or above threshold $g_{avg} = 0$,. Moreover, at EP, $\Omega_\pm = \omega_{avg}$. By recalling that $\omega_2 = \omega_1 + 2K\alpha$ and that the lasing condition $g_1 = -g_2$ implies that $\sum_{j=1}^{2}(n_j - n_0)\beta\Gamma_\parallel = 2\kappa$, we find:

$$\Omega_{EP} = \omega_1 + \alpha(\kappa + K) \tag{S17}$$

S4. LIGHT-IN LIGHT-OUT CURVE

We experimentally measure the light-in vs light-out curve of our sample when two cavities are solely pumped (see Fig. S3). Note that the difference between two curves is caused by the alignment of the cavity, i.e., the spectrometer is aligned with respect to one of the cavities.

S5. STABILITY OF THE SOLUTIONS

To calculate lasing modes and their bifurcation diagrams, we express the complex fields as $a_j = A_j(t)e^{i\omega t + i\phi_j(t)}$. By substituting back in the laser rate equations (Eq.(1a) in the main text) we obtain:

$$\dot{A}_1 = \frac{1}{2}\left[\beta\Gamma_\parallel(n_1 - n_0) - 2\kappa\right]A_1 + KA_2\sin\Delta\phi, \tag{S18}$$

$$\dot{A}_2 = \frac{1}{2}\left[\beta\Gamma_\parallel(n_2 - n_0) - 2\kappa\right]A_2 - KA_1\sin\Delta\phi, \tag{S19}$$

$$\begin{aligned}\dot{\Delta\phi} \equiv \dot{\phi}_1 - \dot{\phi}_2 = \frac{1}{2}\alpha\beta\Gamma_\parallel(n_1 - n_0) + \frac{A_2}{A_1}K\cos\Delta\phi - \\ \left[\frac{1}{2}\alpha\beta\Gamma_\parallel(n_2 - n_0) + \frac{A_1}{A_2}K\cos\Delta\phi\right] + \delta\omega.\end{aligned} \tag{S20}$$

The lasing modes and their bifurcation diagrams are then calculated by solving these equations together with the carrier rate equations (Eq.(1b) in the main text) by using the open source continuation software package MatCont [1]. Accessing a particular mode using numerical integration of the laser equations can be achieved by choosing the proper initial noise in the system.

The stability of the modes are calculated by using linear stability analysis around the lasing modes, i.e. using the Jacobian matrix:

$$\boldsymbol{J} = \begin{bmatrix} \frac{\partial f_{A_1}}{\partial A_1} & \frac{\partial f_{A_1}}{\partial A_2} & \frac{\partial f_{A_1}}{\partial n_1} & \frac{\partial f_{A_1}}{\partial n_2} & \frac{\partial f_{A_1}}{\partial \Delta\phi} \\ \frac{\partial f_{A_2}}{\partial A_1} & \frac{\partial f_{A_2}}{\partial A_2} & \frac{\partial f_{A_2}}{\partial n_1} & \frac{\partial f_{A_2}}{\partial n_2} & \frac{\partial f_{A_2}}{\partial \Delta\phi} \\ \frac{\partial f_{n_1}}{\partial A_1} & \frac{\partial f_{n_1}}{\partial A_2} & \frac{\partial f_{n_1}}{\partial n_1} & \frac{\partial f_{n_1}}{\partial n_2} & \frac{\partial f_{n_1}}{\partial \Delta\phi} \\ \frac{\partial f_{n_2}}{\partial A_1} & \frac{\partial f_{n_2}}{\partial A_2} & \frac{\partial f_{n_2}}{\partial n_1} & \frac{\partial f_{n_2}}{\partial n_2} & \frac{\partial f_{n_2}}{\partial \Delta\phi} \\ \frac{\partial f_{\Delta\phi}}{\partial A_1} & \frac{\partial f_{\Delta\phi}}{\partial A_2} & \frac{\partial f_{\Delta\phi}}{\partial n_1} & \frac{\partial f_{\Delta\phi}}{\partial n_2} & \frac{\partial f_{\Delta\phi}}{\partial \Delta\phi} \end{bmatrix} \tag{S21}$$

where f_ξ defined as $\dot{\xi} = f_\xi(A_1, A_2, n_1, n_2, \Delta\phi)$ (for $\xi = A_j, n_j, \Delta\phi$), represent the fixed points of the nonlinear dynamical equations, namely $\dot{\xi} = 0, \dot{n_j} = 0, \dot{\Delta\phi} = 0$. Negative and positive values of the real part of the complex eigenvalues of the Jacobian then indicate stable and unstable solutions, respectively.

Interestingly, the bifurcation diagrams in the main text and supplementary show that there exist a regime around the bifurcation point where all the fixed points are unstable. As illustrated in Figure. (S4), which is calculated for $P_{tot} = 3.5P_0$, the system does not admit stable steady state solutions but rather oscillates in time.

S6. STOCHASTIC ANALYSIS OF LASER RATE EQUATIONS

In the main text, we presented a comparison between the experimental results and numerical simulations obtained by solving the laser rate equations in the presence of stochastic noise. In general, there are different algorithms for integrating stochastic differential equations. Here we employed the Eurler-Maruyama method [2]. The noise terms, which arise due spontaneous emission, was taken to be a white noise: $\langle F_\mu(t)F_\nu(t')\rangle = 2D_{\mu\nu}\delta(t - t')$. The coefficient is $2D_{a_i a_i^*} = 2D_{a_i a_i^*} = R_{sp}$, with R_{sp} being the spontaneous emission rate $R_{sp} = \beta F_p B n_{1,2}^2/V_a$, where F_p is Purcell factor, B is the bimolecular radiative

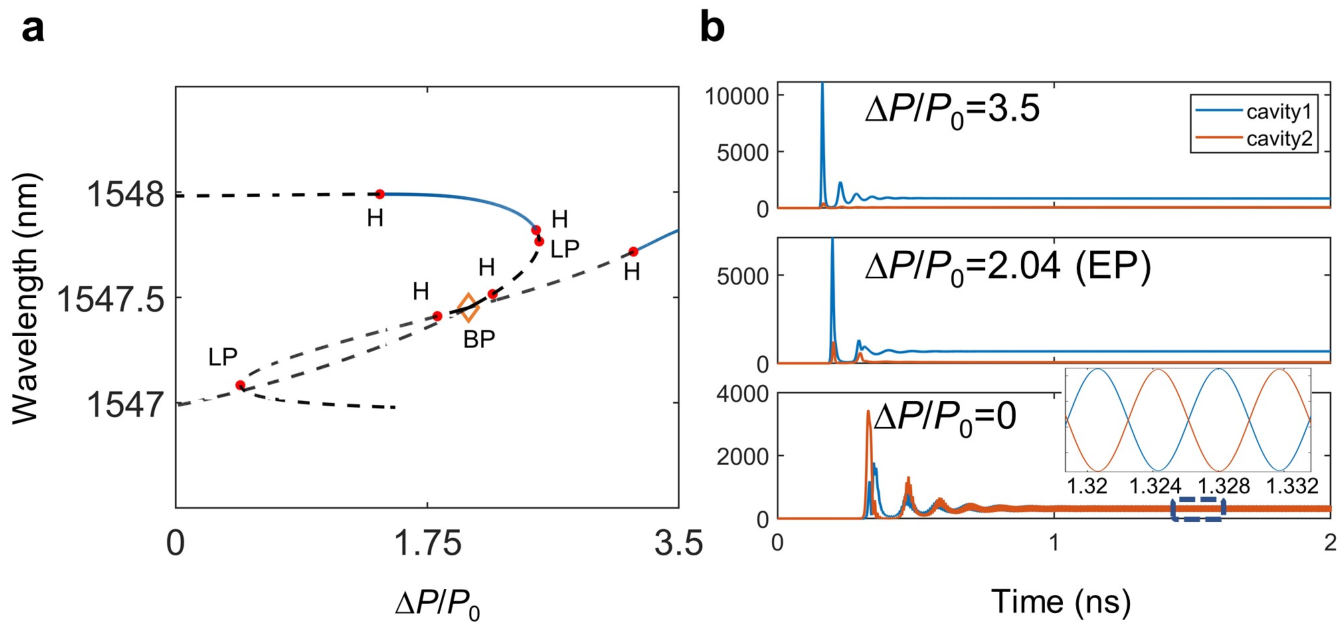

FIG. S4. **a** Bifurcation diagram and stability calculated for $P_{tot} = 3.5P_0$. **b** Temporal dynamics for an exemplary stable solutions (top and middle panel) and one unstable, oscillator, solution (bottom panel).

recombination rate and V_a is the volume of the active medium [3]. The spectra are obtained after the Fourier transformation of the numerical integration. The numerical values of parameters used in the simulations are listed in table S1.

TABLE S1. Parameter values

Symbol	Values
κ	140.86GHz
α	3
β	0.017
$\Gamma_{\parallel}$	2.2GHz
$\Gamma_{\rm tot}$	5GHz
V_a	0.016×10^{-12}cm^3
F_p	1.03
B	$3{\times}10^{10}$ cm^{3}s^{-1}

S7. EXTENDED DATA

For completeness, in this section, we present more measurement data for the lasing mode wavelengths as a function of $\Delta P \in [-1, 1]$ evaluated at different values of P_{tot}. These results are plotted in Fig.S5. By tracking the location of the bifurcation point in each figure, it is clear that the trend discussed in the main text (i.e. the shift of the bifurcation point toward larger negative values of ΔP as P_{tot} increased does persist. On the other hand, Fig.S6 depicts the experimental (top row) and numerical (lower row) results for the lasing characteristics of this system in the absence of frequency detuning compensation. In this case, there is no EP in the system and the lasing characteristics are considerably less sensitive to the total pump power.

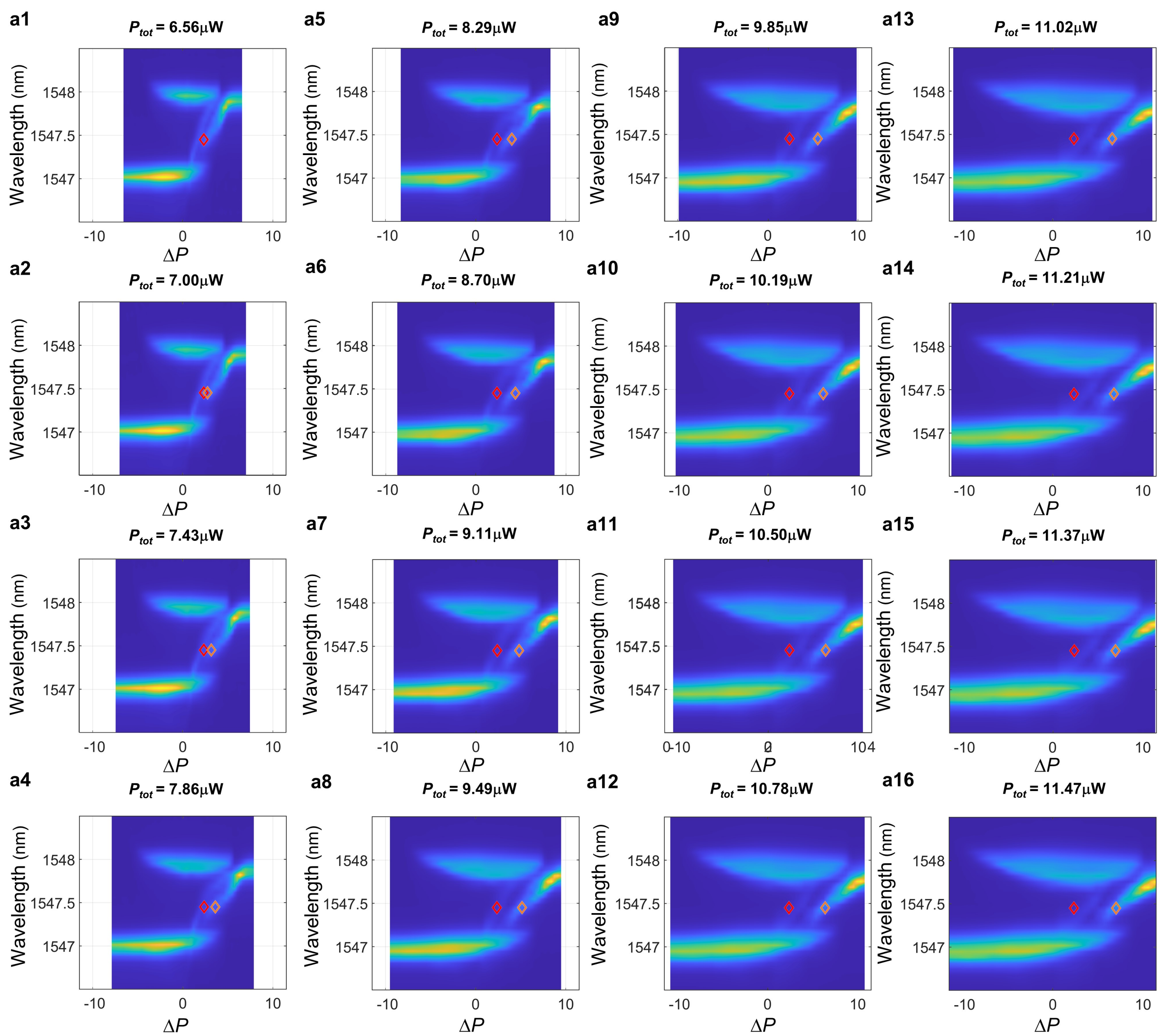

FIG. S5. Extended data for the measurements of the lasing modes as a function of ΔP for different values of P_{tot}. The same trend discussed in the main text is observed here as well, which supports the conclusion of this work.

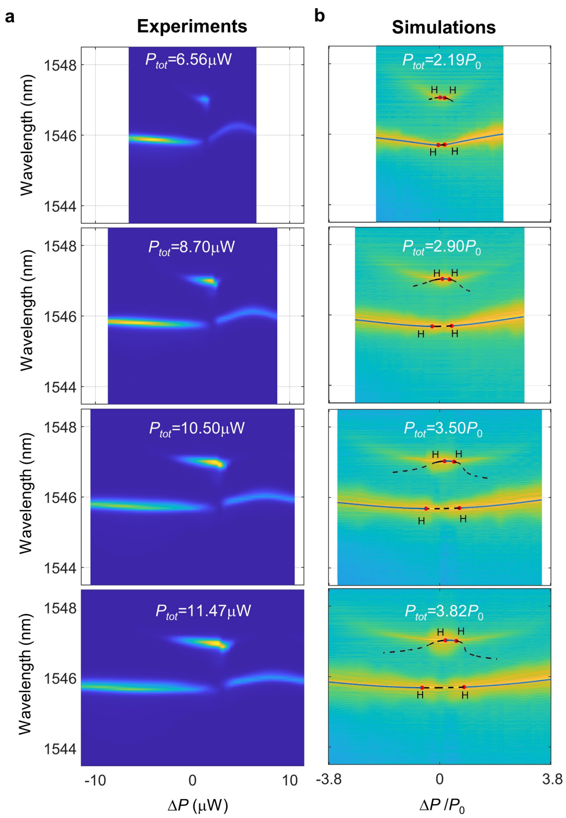

FIG. S6. Similar measurements to those presented in Fig.3 in the main text but for a different sample having $\delta\omega = 1.19 \ll 2g\alpha = 22.38$ ($g = 3.73$), i.e. with no frequency compensation to counterbalance the carrier-induced blueshift. As before, left panels present experimental data while right panels depicts theoretical results. In contrast to the behavior observed in Fig. 3 in the main text, here the lasing spectral pattern remains almost invariant as the total pump power is varied.

[1] A. Dhooge, W. Govaerts, Y. A. Kuznetsov, H. G. E. Meijer, and B. Sautois, Mathematical and Computer Modelling of Dynamical Systems **14**, 147 (2008).

[2] P. E. Kloeden and E. Platen, in *Numerical solution of stochastic differential equations* (Springer, 1992) pp. 103–160.

[3] M. Marconi, F. Raineri, A. Levenson, A. M. Yacomotti, J. Javaloyes, S. H. Pan, A. El Amili, and Y. Fainman, Physical Review Letters **124**, 213602 (2020).